The Astrophysical Journal, 850:73 (10pp), 2017 November 20 https://doi.org/10.3847/1538-4357/aa917c

Probing the EBL Evolution at High Redshift Using GRBs Detected with the *Fermi*-LAT

A. Desai[1], M. Ajello[1], N. Omodei[2], D. H. Hartmann[1], A. Domínguez[3], V. S. Paliya[1], K. Helgason[4], J. Finke[5], and M. Meyer[6]
[1] Department of Physics and Astronomy, Clemson University, Kinard Lab of Physics, Clemson, SC 29634-0978, USA
abhishd@g.clemson.edu, majello@g.clemson.edu
[2] W. W. Hansen Experimental Physics Laboratory, Kavli Institute for Particle Astrophysics and Cosmology, Department of Physics and SLAC National Accelerator Laboratory, Stanford University, Stanford, CA 94305, USA; nicola.omodei@stanford.edu
[3] Grupo de Altas Energías, Universidad Complutense de Madrid, E-28040 Madrid, Spain
[4] Max-Planck-Institut für Astrophysik, Postfach 1317, D-85741 Garching, Germany
[5] Space Science Division, Naval Research Laboratory, Washington, DC 20375-5352, USA
[6] Stockholm University, SE-106 91 Stockholm, Sweden
Received 2017 March 8; revised 2017 September 28; accepted 2017 October 3; published 2017 November 17

Abstract

The extragalactic background light (EBL), from ultraviolet to infrared wavelengths, is predominantly due to emission from stars, accreting black holes and reprocessed light due to Galactic dust. The EBL can be studied through the imprint it leaves, via γ–γ absorption of high-energy photons, in the spectra of distant γ-ray sources. The EBL has been probed through the search for the attenuation it produces in the spectra of BL Lacertae (BL Lac) objects and individual γ-ray bursts (GRBs). GRBs have significant advantages over blazars for the study of the EBL especially at high redshifts. Here we analyze a combined sample of 22 GRBs, detected by the *Fermi* Large Area Telescope between 65 MeV and 500 GeV. We report a marginal detection (at the $\sim 2.8\sigma$ level) of the EBL attenuation in the stacked spectra of the source sample. This measurement represents a first constraint of the EBL at an effective redshift of $\sim$1.8. We combine our results with prior EBL constraints and conclude that *Fermi*-LAT is instrumental to constrain the UV component of the EBL. We discuss the implications on existing empirical models of EBL evolution.

Key words: cosmology: observations – galaxies: high-redshift – gamma-ray burst: general – gamma-rays: observations – gamma-rays: theory

1. Introduction

Light emitted by stars and accreting compact objects, through the history of the universe, is encoded in the intensity of the extragalactic background light (EBL). Cosmic dust in the vicinity of these sources absorbs some fraction of their light and reemits it in the infrared part of the electromagnetic spectrum. The resulting multi-component spectral energy density is a function of redshift, determined by cosmological parameters, stellar initial mass function, the cosmic star formation rate history and the dust content in galaxies (Hauser & Dwek 2001; Kashlinsky 2005a). Therefore, an understanding of the EBL evolution allows us to probe these astrophysical ingredients. In addition to these standard sources of light, the EBL could also comprise photons from dark matter particle decay and other potential exotic energy releases (Maurer et al. 2012; Domínguez & Prada 2013). The evolving EBL in the high-redshift domain ($z \gtrsim 6$) is of particular importance, as it traces the reionization epoch (Inoue et al. 2014). Contributions from the first generation of stars (Pop III), might have originated from very massive stars, which cannot be observed directly with present day observatories or even with the soon to be launched James Webb Telescope. These topics have been discussed widely in the literature (Bond et al. 1986; Dwek et al. 2005; Kashlinsky et al. 2005, 2012; Raue et al. 2009; Gilmore 2012; Inoue et al. 2013; Dwek 2014).

Recognizing the importance of the EBL and its evolution with redshift, many efforts have been made to measure its photon intensity. Indeed, direct measurements of the EBL are difficult because of the bright foregrounds like Galactic emission and zodiacal light (Hauser et al. 1998; Matsumoto et al. 2005; Matsuoka et al. 2011; Mattila et al. 2017), resulting in estimates of the intensity of the EBL that are up to a factor of 10 larger than lower limits obtained by integrating the light of galaxies resolved in deep surveys (Madau & Pozzetti 2000; Keenan et al. 2010; Driver et al. 2016). Studies of background fluctuations in the EBL suggest lower, though nonzero, levels of unresolved EBL intensity (Kashlinsky et al. 2012; Zemcov et al. 2014).

An indirect approach of probing the EBL and its redshift evolution is through the γ–γ absorption it imprints in the spectra of distant high-energy γ-ray sources. The high-energy part of their spectral energy distributions (SEDs) is attenuated due to annihilation with background photons (γ–$\gamma \Rightarrow e^+$–e^- pair creation) as discussed by Nikishov (1961) and Gould & Schréder (1967a, 1967b). Because of the shape of the pair-production cross section, γ rays (of a given energy) will most likely interact with EBL photons of given wavelengths: e.g., γ-rays with $E \gtrsim 50$ GeV (and from $z \gtrsim 1$) are attenuated mainly by photons of the optical-UV background (>1 eV). The total optical depth to a source is then found from a proper cosmological integration over redshift, which requires an understanding of how the EBL builds up with cosmic time (Dwek & Krennrich 2013).

This extinction process therefore allows the use of γ rays of different energies (and originating from sources at different redshifts) to explore the SED of the EBL and its evolution with redshift. While the Galactic emissions and zodiacal light constitute a problem for direct measurements, they make no difference for the γ-ray technique as the mean free path of photons in the MeV to TeV regime is much larger

Table 1
GRB Used for Analysis (GRBs Are Sorted Increasingly by the Time of the Event)

GRB Name	Date (MST)	R.A. Deg., J2000.0	Decl. Deg., J2000.0	Redshift	*T* Start (UTC)	Duration Seconds[a]	Flux (10^{-5})[b] ph cm^{-2} s^{-1}	Photon Index[b]	TS[b]
080916C	2008 Sep 16	119.85	−56.60	4.35	00:12:45.6	1775.9	7.89 ± 0.49	2.25 ± 0.06	1140.7
090323	2009 Mar 23	190.71	17.10	3.57	00:02:42.6	5615.9	1.42 ± 0.19	2.28 ± 0.13	205.0
090328	2009 Mar 28	90.67	−42.00	0.74	09:36:46.5	7485.6	0.52 ± 0.07	2.10 ± 0.11	253.6
090510	2009 May 10	333.55	−26.60	0.90	00:22:59.9	177.8	34.11 ± 2.11	2.05 ± 0.05	1234.6
090902B	2009 Sep 2	264.94	27.32	1.82	11:05:08.3	749.5	14.32 ± 0.70	1.91 ± 0.04	2219.0
090926A	2009 Sep 26	353.40	−66.32	2.11	04:20:26.9	4889.3	4.61 ± 0.28	2.08 ± 0.05	1267.2
091003	2009 Oct 3	251.52	36.63	0.90	04:35:45.5	451.6	2.17 ± 0.40	2.04 ± 0.15	192.3
100414A	2010 Apr 14	192.11	8.69	1.37	02:20:21.9	5622.5	0.39 ± 0.07	1.77 ± 0.11	188.8
100728A	2010 Jul 28	88.76	−15.26	1.57	02:17:30.6	693.7	0.65 ± 0.19	1.92 ± 0.21	69.9
110731A	2011 Jul 31	280.50	−28.54	2.83	11:09:29.9	561.3	3.20 ± 0.45	2.22 ± 0.12	194.3
120624B	2012 Jun 24	170.87	8.93	0.57	22:23:53.0	1104.3	3.86 ± 0.35	2.46 ± 0.10	456.3
120711A	2012 Jul 11	94.69	−71.00	1.41	02:44:53.0	5307.2	0.56 ± 0.12	1.93 ± 0.15	136.7
130427A	2013 Apr 27	173.14	27.71	0.34	07:47:6.0	10000	4.19 ± 0.18	1.99 ± 0.03	2755.8
130518A	2013 May 18	355.67	47.47	2.49	13:54:37.0	302.9	5.38 ± 0.94	2.54 ± 0.19	106.0
130702A	2013 Jul 2	217.31	15.77	0.15	00:05:23.0	384.5	0.04 ± 0.02	1.56 ± 0.32	42.8
130907A	2013 Sep 7	215.89	45.61	1.24	21:42:19.0	16600	0.91 ± 0.56	2.10 ± 0.46	12.8
131108A	2013 Nov 8	156.50	9.66	2.40	20:41:55.0	1333.5	4.52 ± 0.32	2.63 ± 0.09	559.0
131231A	2013 Dec 31	10.59	−1.65	0.62	04:45:16.1	5605.6	0.34 ± 0.07	1.73 ± 0.12	229.1
141028A	2014 Oct 28	322.60	−0.23	2.33	10:55:03.08	414.2	2.33 ± 0.50	2.22 ± 0.21	86.7
150314A	2015 Mar 14	126.68	63.83	1.76	04:54:50.0	250	2.24 ± 0.88	2.66 ± 0.41	19.4
150403A	2015 Apr 3	311.51	−62.71	2.06	21:54:10.9	1678.3	0.22 ± 0.08	1.87 ± 0.23	42.1
150514A	2015 May 14	74.88	−60.91	0.81	18:35:05.4	600	0.09 ± 0.07	1.30 ± 0.42	28.3

Notes.
[a] Duration of the GRB considered for our analysis.
[b] Parameters obtained from the analysis described in Section 2.

Table 2
Photons Detected by the *Fermi*-LAT at an Optical Depth Greater Than 0.1

GRB Name	Redshift	Number of Photons Finke et al. (2010)[a]	Number of Photons Domínguez et al. (2011)[b]	Number of Photons Kneiske & Dole (2010)[c]	Corresponding Energy of Photons (GeV)[d]
080916C	4.35	2	0	2	12.4, 27.4
090323	3.57	0	0	0	⋯
090328	0.74	0	0	0	⋯
090510	0.90	0	0	0	⋯
090902B	1.82	2	0	2	39.9, 21.7
090926A	2.11	1	0	1	19.5
091003	0.90	0	0	0	⋯
100414A	1.37	1	0	2	29.8
100728A	1.57	0	0	0	⋯
110731A	2.83	0	0	0	⋯
120624B	0.57	0	0	0	⋯
120711A	1.41	0	0	0	⋯
130427A	0.34	1	3	2	94.1
130518A	2.49	0	0	0	⋯
130702A	0.15	0	0	0	⋯
130907A	1.24	1	0	1	50.9
131108A	2.40	0	0	0	⋯
131231A	0.62	0	0	1	⋯
141028A	2.33	0	0	0	⋯
150314A	1.76	0	0	0	⋯
150403A	2.06	0	0	0	⋯
150514A	0.81	0	0	0	⋯

Notes.
[a] Number of LAT photons detected at $\tau > 0.1$ (obtained using EBL model Finke et al. (2010)—model C).
[b] Upper limit of the number of LAT Photons detected at $\tau > 0.1$ (obtained using the EBL model; Domínguez et al. 2011).
[c] Lower limit of the number of LAT Photons detected at $\tau > 0.1$ (obtained using the EBL model; Kneiske & Dole 2010).
[d] Energy of the photons detected at $\tau > 0.1$ (obtained using the EBL model; Finke et al. 2010—model C).

(>10 Mpc) than Galactic or solar scales (Adams et al. 1997). Observations over the $0.2 < z < 1.6$ redshift range with the *Fermi* Large Area Telescope (LAT) have resulted in the detection of the EBL attenuation in a collective sample of 150 BL Lacertae objects (BL Lacs, see Ackermann et al. 2012). Ground-based measurements of low-redshift blazars ($z \lesssim 0.6$) in the TeV regime have resulted in optical depth estimates using High Energy Spectroscopic System (H.E.S.S.), Major Atmospheric Gamma Imaging Cherenkov Telescopes (MAGIC) and Very Energetic Radiation Imaging Telescope Array System (VERITAS) data (e.g., Abramowski et al. 2013; Domínguez et al. 2013; Biteau & Williams 2015). All measurements in the $0 \lesssim z \lesssim 1.6$ range point to a level of the UV-to-NIR EBL that is compatible with that inferred from galaxy counts as estimated by recent models (e.g., Franceschini et al. 2008; Finke et al. 2010; Domínguez et al. 2011; Helgason & Kashlinsky 2012; Stecker et al. 2012, 2016).

All measurements of the γ-ray opacity measured above rely on BL Lacs as probes of the EBL. Because it has been proposed that the observed γ-ray absorption may be affected by a line-of-sight interaction with cosmic rays (accelerated in jets of BL Lacs) producing secondary γ-rays, there remain some doubts whether γ-ray measurements of the EBL using blazars are trustworthy (Essey & Kusenko 2010; Essey et al. 2011). Line-of-sight interaction of cosmic rays (accelerated in jets of BL Lacs) with the CMB/EBL would generate a secondary γ-ray component, which, being much closer to the observer would suffer less EBL attenuation and would lead to underestimation of the true EBL energy density. The detection at TeV energies of BL Lacs with unusually hard de-absorbed spectra (e.g., Horns & Meyer 2012; Furniss et al. 2013) has been interpreted also in this framework. These possibilities were discounted by Biteau & Williams (2015) who find that the spectra reconstructed after de-absorption are not too hard with respect to expectations. A similar conclusion was reached by Domínguez & Ajello (2015) who do not find any deviation of the predicted EBL attenuation in the LAT blazar data. In addition to these theoretical uncertainties, the sample of BL Lacs suffers from a significant drop in sample size beyond a redshift of ∼1.0.

In this work, we overcome these limitations using the γ-ray bursts (GRBs) detected by the LAT during a seven-year period and for which redshift measurements are available (Hartmann 2007). The short duration of the bursts ensures that the observed γ-ray emission is generated locally at the source, which renders GRBs clean probes of the EBL. Furthermore, GRBs are also observed at much larger redshifts (i.e., $z = 4.3$ for GRB 089016C as reported by Greiner et al. 2009) thus expanding the study of EBL attenuation to larger distances (see, e.g., Kashlinsky 2005b).

This paper is organized as follows. Section 2 presents the data processing and analysis, Section 3 reports the methodology and results of the EBL study, Section 4 considers systematic effects of the methodology, while Section 5 discusses the results.

2. Data Analysis

There are more than 130 GRBs detected by *Fermi*-LAT (Vianello et al. 2016), out of which 22 GRBs measured between 2008 September and 2015 June have an associated redshift measurement, which comprise our source sample. These GRBs are reported in Table 1 along with their

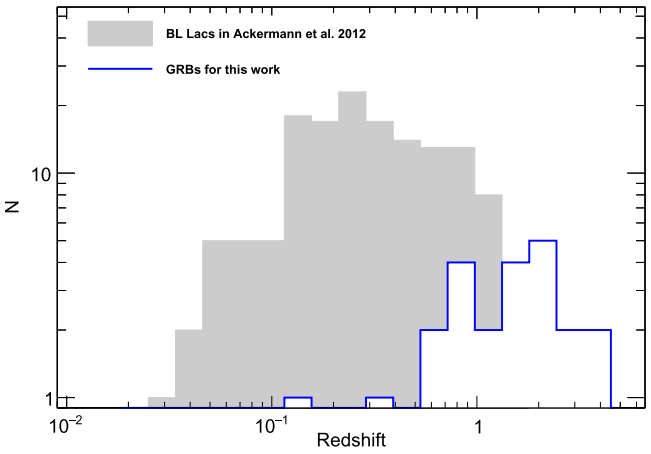

Figure 1. Redshift distribution for the sample of 22 GRBs used here compared to the sample of 150 BL Lacs used in Ackermann et al. (2012).

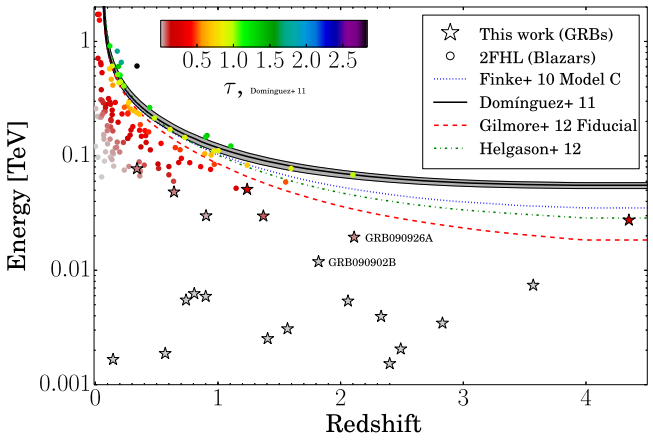

Figure 2. Prediction of the cosmic γ-ray horizon (i.e., the redshift and energy at which $\tau_\gamma\gamma = 1$) from different models (see the legend) along with the highest energy photons from AGNs and GRBs at different redshifts. The GRBs from our sample are denoted by stars and AGNs by dots, while the estimates from EBL models are denoted by lines. The two most constraining GRBs in our analysis are labeled in the plot for reference.

corresponding parameters. Table 2 reports the number of photons detected with the *Fermi*-LAT at an EBL optical depth greater than 0.1 (obtained using the model of Finke et al. (2010)—model C and corresponding redshift measurement for each GRB). In order to show how much the number of photons above a given optical depth varies when the EBL model is changed, we also report the number of photons detected at $\tau > 0.1$ using the models of Domínguez et al. (2011) and Kneiske & Dole (2010; a more transparent and more opaque model than the one of Finke et al. 2010 respectively). The redshift distribution for our sample ranges from 0.15 to 4.35 and is shown in Figure 1 compared to the distribution for BL Lacs from the sample used by Ackermann et al. (2012). Figure 2 shows the highest energy photons detected from these GRBs together with the prediction of the cosmic γ-ray horizon from different models.

For each GRB, we extract transient-class Pass 8 photons detected with the *Fermi*-LAT between 65 MeV and 500 GeV within 10° of the source. The start time (in UTC) and duration of each burst (reported in Table 1) is obtained from the LAT first GRB catalog (Ackermann et al. 2013b), the online GRB table,[7] and individual burst papers (Abdo et al. 2009b; de Palma et al. 2009; Kumar & Barniol Duran 2010; Ackermann et al. 2011; Tam et al. 2013). There are no diffuse models available at energies less than 65 MeV and the effective area of *Fermi*-LAT decreases steeply at low energies, reducing the overall sensitivity. So, to obtain maximum signal strength, we took 65 MeV as the lower limit for the analysis. The maximal energy must be $\gtrsim$10 GeV, as photons having energy greater than 10 GeV interact with the EBL to produce electron–positron pairs. The universe is transparent below ~10 GeV (Stecker et al. 2006), meaning that the measured spectrum will be equal to the intrinsic spectrum for $E < 10$ GeV. To retain sensitivity to EBL attenuation, we adopt 500 GeV as the upper limiting energy.

The burst data for each GRB are analyzed using *Fermi Science-Tools* (version v10r0p5).[8] These data are filtered, removing the photons having a zenith angle greater than 105°, to limit the contamination due to Earth's limb (this analysis is robust against changes in zenith angle cuts).[9] The photons collected by the LAT when it is in the South Atlantic Anomaly are also filtered out. The spectral analysis of the burst is done by an unbinned likelihood maximization of a sky model created for each GRB. The sky model consists of a central point source, the GRB, whose spectrum is modeled as a power law, and the diffuse (Galactic and isotropic) models. The Galactic and isotropic models are modeled using the gll_iem_v06.fits and iso_P8R2_TRANSIENT020_V6_v06.txt templates[10] respectively (Acero et al. 2016). We use the *P8R2_TRANSIENT*020 instrument response function.

The Minuit[11] optimizer is used to determine the best-fit spectral parameters and the error estimate for the unbinned likelihood maximization analysis. GRB spectra are generally described using the "Band function" (Band et al. 1993), which consists of two power laws joined by a exponential cut-off, or a Comptonized model, which consists of a power law with exponential cut-off (Ackermann et al. 2013c). According to Ackermann et al. (2013c) and Vianello et al. (2015), the "Band function" alone is inadequate to model GRB spectra over the keV–GeV energy range observed by *Fermi* and a power-law component is required in all bright LAT bursts to account for the high-energy data (>100 MeV). This component may be produced by synchrotron radiation resulting in a power-law-like spectrum (as reported by Tam et al. 2013 and discussed also by Kumar & Barniol Duran 2009, 2010; Ghisellini et al. 2010; Wang et al. 2010). We thus approximate the intrinsic spectrum of GRBs with a power law and assess in Section 4.2 how well this assumption works.

The power law used for our intrinsic point source spectra is given by

$$\frac{dN_0}{dE} = \frac{N_0(\alpha+1)E^{\alpha}}{E_{\rm max}^{\alpha+1} - E_{\rm min}^{\alpha+1}}, \quad (1)$$

where N_0 gives the normalized flux in units of $\rm cm^{-2}\,s^{-1}\,MeV^{-1}$ between $E_{\rm min}$ and $E_{\rm max}$ taken as 65 MeV and 500 GeV, respectively, while α is the photon index. For the likelihood analysis of each GRB, three parameters (N_0 and α of the point

[7] http://fermi.gsfc.nasa.gov/ssc/observations/types/grbs/lat_grbs/table.php
[8] http://Fermi.gsfc.nasa.gov/ssc/data/analysis/scitools/
[9] Adopting a more stringent zenith angle cut of 85° produces negligible impact on our analysis.
[10] http://Fermi.gsfc.nasa.gov/ssc/data/access/lat/BackgroundModels.html
[11] http://lcgapp.cern.ch/project/cls/work-packages/mathlibs/minuit/doc/doc.html

Table 3
Joint-likelihood Results for Different EBL Models Using GRB Sources

Model	TS_0[a]	p_0[b]	b[c]	TS_1[d]	p_1[b]	ΔTS[e]
Kneiske et al. (2004)—high UV	6.5	2.55	$0.43^{+0.24}_{-0.28}$	3.5	1.87	3.0
Kneiske et al. (2004)—best-fit	7.4	2.72	$0.80^{+0.51}_{-0.61}$	0.1	0.32	7.3
Primack et al. (2005)	4.7	2.17	$0.51^{+0.34}_{-0.38}$	1.5	1.22	3.2
Gilmore et al. (2009)	7.1	2.66	$1.25^{+0.82}_{-0.95}$	0.1	0.32	7.0
Finke et al. (2010)—model C	7.7	2.77	$1.27^{+0.84}_{-0.99}$	0.1	0.32	7.6
Kneiske & Dole (2010)	7.4	2.72	$1.29^{+0.80}_{-0.95}$	0.2	0.45	7.2
Domínguez et al. (2011)	8.0	2.83	$2.21^{+1.48}_{-1.83}$	1.0	1.00	7.0
Gilmore et al. (2012)—fixed	7.3	2.70	$1.43^{+0.93}_{-1.13}$	0.3	0.55	7.0
Gilmore et al. (2012)—fiducial	6.5	2.55	$0.63^{+0.40}_{-0.46}$	0.7	0.84	5.8
Helgason & Kashlinsky (2012)	7.2	2.68	$1.44^{+0.95}_{-1.18}$	0.3	0.55	6.9
Scully et al. (2014)—low opacity	6.9	2.62	$1.16^{+0.69}_{-0.79}$	0.1	0.32	6.8
Scully et al. (2014)—high opacity	6.7	2.59	$0.42^{+0.25}_{-0.29}$	3.3	1.82	3.4
Inoue et al. (2013)	6.4	2.53	$0.72^{+0.43}_{-0.50}$	0.4	0.63	6.0

Notes.
[a] TS obtained from the comparison of the null hypothesis ($b = 0$) with the likelihood obtained with best-fit value for b.
[b] The p_0 and p_1 values are denoted in units of standard deviation of a normal Gaussian distribution.
[c] This column lists the best-fit values and 1σ confidence ranges for the opacity scaling factor.
[d] Here the compatibility of the predictions of EBL models with the *Fermi* observations is shown ($b = 1$ case constitutes the null hypothesis). Large values mean less likely to be compatible.
[e] $\Delta TS = TS_0 - TS_1$.

source and the normalization of the isotropic diffuse source) are left free to vary while the rest are fixed. Because of the short time integration of bursts and lack of photons to constrain both background emissions, the Galactic diffuse emission is fixed. The log likelihood value obtained from the null case (LL_{null}), where the source is not present, is compared with the log likelihood value obtained from the source model (LL) using the Test Statistic (TS) given by $2(LL - LL_{null})$. The TS value along with the estimated flux and photon index are reported, for all GRBs, in Table 1. The source significance, which gives us the confidence level for the detection of each GRB, is obtained by taking the square root of the TS value $n_\sigma = TS^{1/2}\sigma$ (Mattox et al. 1996).

3. EBL Study

3.1. Likelihood Methodology

Our EBL analysis aims to find out the attenuation due to the EBL in the spectra of GRBs. To measure the EBL attenuation, in this work, we test separately the normalization and shape of optical depth curves predicted by several EBL models. The normalization of the optical depth is tested following a procedure similar to that of Ackermann et al. (2012) by performing the likelihood ratio test (see also Abramowski et al. 2013 and Ahnen et al. 2016), while the shape is tested as discussed in Section 5. Owing to the limited signal-to-noise ratio of the measurement within the considered energy range, the shapes of most EBL models are found to be similar to each other (also discussed in Section 5). This similarity makes the LAT data more sensitive to the normalization than to the shape of the models. Moreover, this approach is compatible (and allows for an easy comparison) with the method adopted also by, e.g., MAGIC, H.E.S.S, and VERITAS (Orr 2011; Abramowski et al. 2013; Mazin et al. 2017). The EBL absorption is parametrized as $e^{-b\cdot\tau_{\rm model}}$, where the optical depth $\tau_{\rm model} = \tau(E, z)$ is derived by 13 EBL models (see Table 3, e.g., Kneiske et al. 2004; Finke et al. 2010; Domínguez et al. 2011; Helgason & Kashlinsky 2012; Stecker et al. 2012) and depends on the photon energy E and source redshift z under consideration. This EBL optical depth is scaled to fit the data using the b parameter. The observed spectrum is then given by

$$F(E)_{\rm observed} = F(E)_{\rm intrinsic} \cdot e^{-b\cdot\tau_{\rm model}} \quad (2)$$

where, $F(E)_{\rm intrinsic} = dN_0/dE$ gives the intrinsic GRB spectrum.

A stacking analysis is used to determine the significance of the EBL attenuation in the observed GRB spectra and to overcome the limitation of low statistics from single GRB sources. In this analysis, the best-fit value of the scaling parameter b is determined through a simultaneous fit to all GRBs. The spectral parameters of each GRB were allowed to vary independently during the fitting with the exception of b (i.e., the scaled EBL attenuation is common to all GRBs), while the parameter of the isotropic component is fixed at its best-fitting value (found analyzing each single ROI) and those of the Galactic model are kept fixed at their nominal, nonoptimized, values. Therefore, a total of 45 parameters are left free to vary (two parameters for each GRB and one parameter given by b).

We define two test statistics TS_0 and TS_1 that are used to assess, respectively, the significance of the EBL detection and the inconsistency of a given EBL model with the LAT data. These are defined as $TS_0 = -2[LL(b_{\rm best\ fit}) - LL(b = 0)]$ and $TS_1 = -2[LL(b_{\rm best\ fit}) - LL(b = 1)]$, where $LL(b_{\rm best\ fit})$, $LL(b = 0)$, and $LL(b = 1)$ are the log-likelihoods of when b was left free to vary, and fixed at 0 and 1 respectively. The TS_0 value is obtained by comparing the null case, which indicates no EBL attenuation, to the best-fit case. The significance is calculated using $\sqrt{TS_0}\sigma$, which gives the confidence level for the detection of the EBL attenuation. The TS_1 value represents a measurement of the significance of the rejection of a given EBL model. A high value will mean that the model is rejected as it predicts an attenuation that is larger than observed, with a significance of the model rejection given by

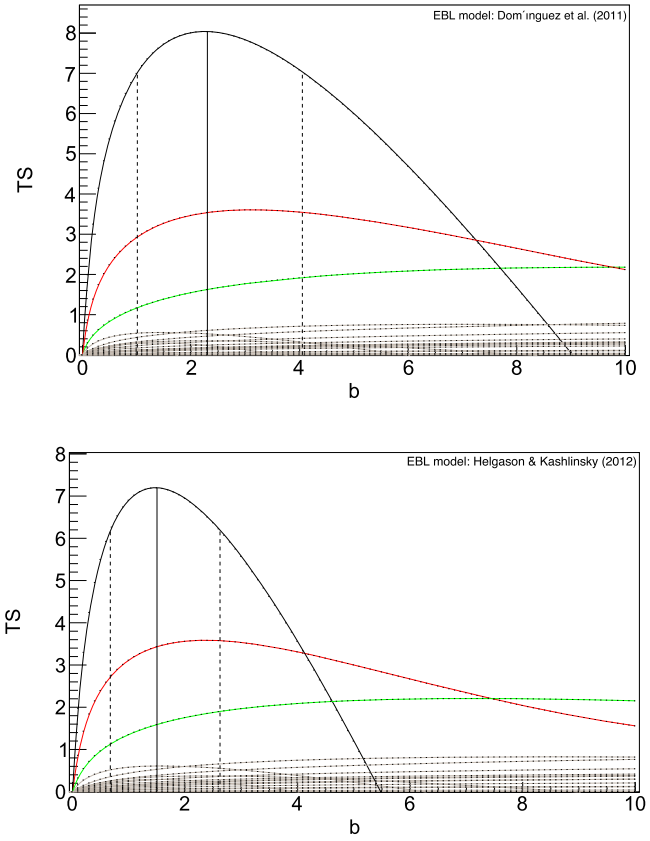

Figure 3. Combined measurement (shown by a solid black line) of the TS_0 values of 22 GRBs as a function of b is displayed for the EBL models of Domínguez et al. (2011; top) and Helgason & Kashlinsky (2012; bottom) along with the measurements for individual GRBs. The solid red and green lines show the maximum contributions to the EBL analysis obtained from GRB 090902B and GRB 090926A, respectively, while the solid gray lines show contributions from the remaining 20 GRB sources. The best-fit value for the scaling parameter with 1σ uncertainty values is also shown by the vertical solid and dashed lines respectively.

$\sqrt{TS_1}\,\sigma$. We also use the TS_0 and TS_1 to calculate the p values of a χ^2 distribution with one degree of freedom using $p = \int_{TS}^{\infty} d\chi^2 \mathrm{PDF}(\chi^2, \mathrm{DOF} = 1)$, where PDF stands for probability density function and DOF stands for degrees of freedom.

3.2. Results

Out of the 13 EBL models tested, the EBL analysis discussed in Section 3.1 gave a maximum TS_0 value of 8.04 for the EBL model of Domínguez et al. (2011) with a best-fit value (with 1σ uncertainty) of $b = 2.21^{+1.48}_{-1.83}$. This rules out the absence of EBL attenuation ($b = 0$) at $\sim 2.8\sigma$ ($p = 4.6 \times 10^{-3}$). The plot of TS_0 for different b values obtained using the Domínguez et al. (2011) model is shown in Figure 3. Note that the major contribution to the TS comes from GRB 090902B and GRB 090926A. If these two bursts are excluded from the analysis, we obtain a $b = 1.3^{+1.91}_{-1.21}$ and $TS_0 = 3.04$ for the model of Domínguez et al. (2011).

The TS_0 and TS_1 values along with the p_0 and p_1 values, which show the EBL detection and model rejection respectively, for all the EBL models tested in this analysis are reported in Table 3. We also report the difference between the significance of detection (TS_0) and the significance of rejection (TS_1). Using the definitions of TS_0 and TS_1, it is easily seen that their difference will be given by $\Delta TS = -2$ [LL

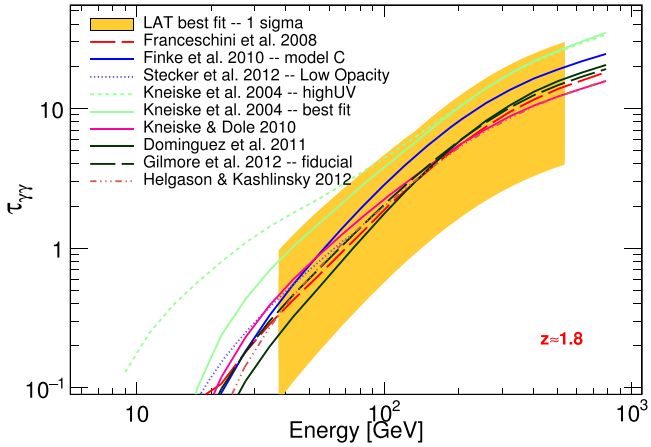

Figure 4. Constraint on the optical depth at a redshift of $z \approx 1.8$, at 1σ confidence level (68%), derived for our GRB sample, compared with model estimates. The models of Franceschini et al. (2008) and Stecker et al. (2012, high and low opacity), not included in the numerical analysis (mentioned in Section 3), are included in the figure for completeness.

$(b = 0) - \mathrm{LL}(b = 1)]$. ΔTS represents the improvement in the fit when the nominal (for a given EBL model) estimate of the EBL attenuation is used with respect to the case of no EBL attenuation. A higher value will imply a more significant detection of the EBL at the level nominally derived by the model being tested. The EBL models accepted by our analysis are the models having TS_1 less than 9, meaning that the model is accepted within a 3σ confidence level. So all the EBL models shown in Table 3 are compatible with the *Fermi*-LAT GRB data. For most of the models, the average TS_0 is around ~ 7.3.

4. Tests for Systematic Effects

4.1. Intrinsic Spectral Curvature

A spectral break was first seen in GRB 090926A at a cut-off energy of ~ 1.4 GeV (Ackermann et al. 2011). Recently, Tang et al. (2015) found six GRBs showing similar spectral features with cut-off energies ranging from ~ 10 to ~ 500 MeV (much lower than the energy at which EBL attenuation takes place). To assess the impact of intrinsic spectral curvature on our EBL analysis, we performed a series of tests modeling the intrinsic source spectrum with a power law with an an exponential cut-off component, modeled as e^{-E/E_C}, dependent on cut-off energy (E_C). The individual source spectrum used for all the GRBs in the likelihood fit is given by

$$\frac{dN}{dE} = N_0 \left(\frac{E}{E_0}\right)^{\gamma} \exp\left(-\frac{E}{E_c}\right), \quad (3)$$

where N_0 is the normalization in units of $\mathrm{cm}^{-2}\,\mathrm{s}^{-1}\,\mathrm{MeV}^{-1}$, γ is the index, E_0 is the scaling energy fixed at 200 MeV and E_C is the cut-off energy. In the source spectrum, N_0, γ, and E_C are left free to vary while for the isotropic diffuse source, the normalization parameter is left free.

In the first test, EBL attenuation is included at the nominal value using Finke et al. (2010), model C, owing to the low uncertainty and high TS_0 values obtained from our analysis. The scaling parameter (b) for the EBL model is fixed at 1. So, in all, four parameters are optimized for each GRB. The maximum likelihood is compared with the likelihood obtained by fixing the cut-off energy at 3 TeV, which is outside the

Table 4
Combined Results of GRB and BL Lac Sources for Different EBL Models

Model[a]	TS_0[b]	p_0[c]	b[d]	TS_1[e]	p_1[c]	ΔTS[f]
Kneiske et al. (2004)—high UV	32.5	5.70	0.38 ± 0.08	38.3	6.19	−5.8
Kneiske et al. (2004)—best-fit	41.0	6.40	0.54 ± 0.12	10.4	3.22	30.6
Primack et al. (2005)	35.0	5.91	0.73 ± 0.14	5.0	2.23	30.0
Gilmore et al. (2009)	40.7	6.38	0.99 ± 0.21	0.1	0.32	40.6
Finke et al. (2010)—model C	41.3	6.43	0.88 ± 0.22	0.3	0.55	41.0
Kneiske & Dole (2010)	39.9	6.32	0.92 ± 0.18	0.19	0.44	39.7
Domínguez et al. (2011)	42.8	6.54	1.04 ± 0.23	0.04	0.20	42.8
Gilmore et al. (2012)—fixed	40.7	6.38	1.04 ± 0.22	0.04	0.20	40.7
Gilmore et al. (2012)—fiducial	40.1	6.33	0.92 ± 0.20	0.16	0.40	39.9

Notes.
[a] Only models common to Ackermann et al. (2012) and our analysis are listed here.
[b] Same as Table 2 but combined TS obtained from GRB and BL Lac observations.
[c] The p_0 and p_1 values are denoted in units of standard deviation of a normal Gaussian distribution.
[d] Maximum likelihood values and uncertainty obtained by performing a weighted average of GRB and BL Lac data.
[e] Same as Table 2 but combined TS obtained from GRB and BL Lac observation.
[f] $\Delta TS = TS_0 - TS_1$.

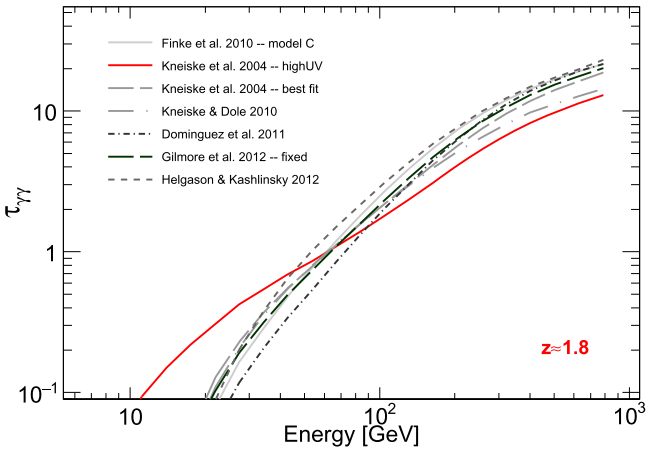

Figure 5. EBL models renormalized to fit the *Fermi*-LAT data. The high-UV model of Kneiske et al. (2004) can be rejected (at 3σ level) on the basis of the shape of its predicted optical depth curve.

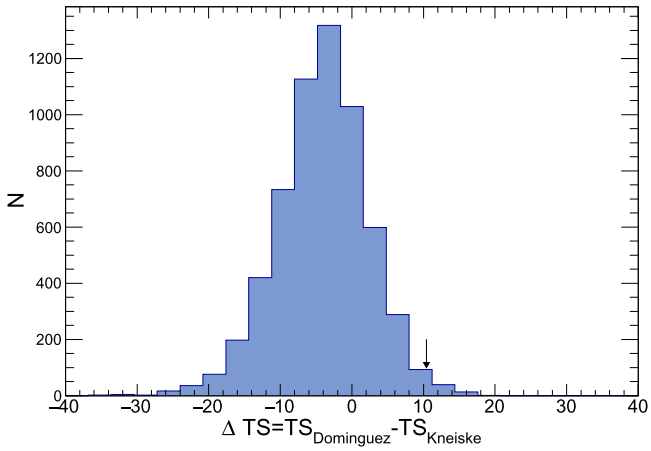

Figure 6. Distribution obtained from simulations of the ΔTS, when comparing the TS_0 of two different models, in the null hypothesis regime. In this case, the simulation adopted the high-UV EBL model of Kneiske et al. (2004). The arrow shows the $\Delta TS = 10.4$ value observed in the real data (see Table 4).

Fermi-LAT energy range and is thus equivalent to having no cut-off in the GRB spectrum (i.e., a simple power-law spectrum). The TS value obtained from this comparison is denoted by TS_C and is used to evaluate the presence of a cut-off in the GRB spectra.

The TS_C value for GRB 090926A is found to be 0.7 from our analysis, which results in a null detection of curvature in the integrated spectrum. This result is different from Ackermann et al. (2011) because we used a longer time interval (4889 s) for the GRB sample as compared to the "prompt" interval (3–21 s) used by Ackermann et al. (2011). A TS_C value greater than 1.9 is found for only 2 of the 22 GRBs in our sample. GRB 120624 has a TS_C value of 3.24 and a best-fit value of 1.23 GeV for the cut-off energy and GRB 131108 has a TS_C value of 4.02 and a best-fit value of 1.13 GeV. The cut-off energies found for both GRBs are significantly lower than the energy at which EBL attenuation takes place, and modeling these two sources as exponentially absorbed power laws has negligible impact on the significance of the detection of the EBL attenuation reported in Table 3.

Second, we repeated the above test, adopting an energy range that is restricted for every GRB so that the EBL attenuation is negligible.[12] In this way, our analysis of the curvature of the GRB intrinsic spectra is not affected by EBL attenuation. This confirms the results of the previous analysis, deriving a TS_C of 3.54 and 4.16 for GRB 120624 and GRB 131108. Again modeling the spectra of these sources to include the exponential cut-off has negligible impact on the EBL.

Third, if the curvature of the intrinsic spectrum were not well modeled (by, e.g., neglecting exponential cutoffs), this effect would be visible as a shift to lower values of the best-fitting b parameter as a function of increasing minimum energy adopted in the analysis. We thus repeated the entire analysis adopting a minimum energy of 1 GeV (instead of 65 MeV) and measured a $TS_0 = 5.9$ and $b = 1.20^{+1.50}_{-0.85}$ for the Finke et al. (2010) model, which is in very good agreement with the results in Table 3. This again shows that modeling the intrinsic GRB spectra with a power law is a reasonable assumption and that

[12] Each spectrum was fitted up to a maximum energy that is derived from each GRB when the attenuation, as predicted from Finke et al. (2010), is negligible (<5%).

intrinsic curvature, if present, is not biasing the result of this analysis.

Finally, we also computed the TS_0 and b values for the Finke et al. (2010) model, modeling all the GRB intrinsic spectra with an exponentially cutoff power law. A TS_0 of 0.87 with a $b = 0.53$ was obtained, which is significantly lower than the result found using a simple power-law model as an intrinsic spectrum for all GRBs (see Table 3). However, this model employs 22 additional free parameters (a cutoff energy per source) while producing a similar log-likelihood as the EBL absorbed power-law model. Model simplicity leads us to prefer the scenario where the power-law emission of GRBs is attenuated by the EBL (a phenomenon already observed in BL Lacs) rather than a more complex intrinsic spectrum. This leads us to conclude that for the EBL analysis using GRBs, a simple power-law spectrum is a reasonable assumption and it is statistically preferred, globally, over an exponentially cutoff power-law spectrum.

4.2. Time Resolved Spectral Analysis

GRBs are known to display substantial spectral evolution during the prompt phase (Zhang et al. 2011; Ackermann et al. 2013a). This calls for an additional time-resolved spectral analysis to justify the usage of time-integrated spectra for the detection of EBL attenuation (Guiriec et al. 2017). We again use Finke et al. (2010), model C, as the EBL model for this test. Again we choose GRB 090902B for this test owing to its relatively high contribution to the TS_0 value. The spectrum of GRB 090902B is created for seven separate time binned intervals obtained from Abdo et al. (2009a). We use a simple power law to model the intrinsic spectrum for each time bin. The process discussed in Sections 2 and 3.1 is followed to obtain TS_0 as a function of b for each time bin. These results are stacked together to obtain a final combined value of $TS_0 = 3.4$ corresponding to a best fit $b = 1.9^{+3.9}_{-1.4}$ in agreement with the time-integrated result of $TS_0 = 3.5$ and $b = 1.8^{+2.8}_{-1.3}$ obtained from Section 3. This agreement shows that using time integrated spectra of GRBs does not have any impact on the detection of the EBL attenuation.

5. Conclusion

The interaction of γ rays from sources at cosmological distances (e.g., GRBs, blazars, radio galaxies, and star-forming galaxies) with EBL photons creates electron–positron pairs causing absorption of γ rays (Stecker et al. 2006). Using *Fermi*-LAT, we searched for the imprint of the EBL in the spectra of 22 GRBs detected by the LAT and for which redshift measurements exist. The low number of photons detected from each single GRB at high energy, predominantly due to the steep decline (with energy) of the LAT effective area, renders the detection of the EBL attenuation in the spectrum of a single source challenging. To overcome this, we analyze the combined set of GRB spectra (stacking), which allows us to reject the null hypothesis of no EBL attenuation at $\sim 2.8\sigma$ confidence.

The constraint on the γ-ray optical depth as derived from this analysis is reported in Figure 4. We report this constraint for an effective redshift of $\sim$1.8. This value is derived by separating the source sample into two redshift bins and finding the value of the redshift separating the bins for which the TS_0 is similar in both bins. This helps us to identify the effective redshift based on the contribution from each GRB. Moreover, dividing the source sample into redshift bins of $0 < z < 1.8$ and $1.8 < z < 4.35$, $TS_0 = 2.45$ for $0 < z < 1.8$ and $TS_0 = 5.78$ for $1.8 < z < 4.35$ are obtained, while dividing it into bins of $0 < z < 1.9$ and $1.9 < z < 4.35$ gives $TS_0 = 5.82$ and 2.18 respectively. This additional test shows that the effective redshift of our sample is $z \approx 1.8$. Also, if GRB090902 at redshift 1.82 is removed from the sample, then the TS values for both the redshift bins are close to equal. This effective redshift is slightly higher than the sample average of 1.63, reflecting the leverage gained by the high-redshift sources in our sample. Figure 4 demonstrates that all the recent EBL models that are in agreement with galaxy counts are also in agreement with the *Fermi*-LAT constraint. The γ-ray horizon ($\tau = 1$) at this effective redshift occurs in the range of 40–180 GeV, consistent with the range found by Domínguez et al. (2011) and Ackermann et al. (2016). As the GRB results are found to be consistent with those derived for BL Lacs, we conclude that secondary γ-rays are not important for moderate optical depths ($\tau \sim 1$), as also argued by Biteau & Williams (2015) and Domínguez & Ajello (2015).

The constraints reported in our analysis can also be combined with those reported by Ackermann et al. (2012) that relied on 150 BL Lacs. These are reported in Table 4. While the baseline model of Stecker et al. (2006) and the "high-UV" model of Kneiske et al. (2004) were already found to be inconsistent with the *Fermi*-LAT BL Lac data, we now find that also the "best-fit" model of Kneiske et al. (2004) is ruled out at the 3σ level when compared to the combined *Fermi*-LAT GRB and BL Lac data.

Photons of energy $\lesssim$100 GeV and from redshift $z > 1$ interact preferentially with photons of the UV background. These deviations are appreciated in Figure 5, which shows the models of Table 4 renormalized to fit the *Fermi* data. It is apparent that all best-fitting (renormalized) models occupy a narrow region of the τ versus energy plot. The optical depth curve predicted by the "high-UV" model of Kneiske et al. (2004) has a shape that is markedly different than the rest of the models, overpredicting the optical depth at <60 GeV and underpredicting it above that energy. This clearly shows that the *Fermi*-LAT offers the capability to probe the UV background at redshifts $\sim$2, a cosmic epoch during which the star formation rate density was near maximum (Madau et al. 1996; Bouwens et al. 2015).

So far studies have been limited to renormalizing the EBL models to fit γ-ray data (Ackermann et al. 2012; Abramowski et al. 2013). This analysis shows that the shape of the optical depth curve of some models may be better than others, even when renormalized to fit the LAT data. For example, the Kneiske et al. (2004)—high UV model implies a significantly different shape, particularly in the UV (and correspondingly 10–50 GeV), as can be seen from Figure 5. In our analysis, we allowed every model to be rescaled by a wavelength-independent factor. Because of the SED shape differences, some models produce significantly better fits than others even after one allows for different renormalization factors. This indicates that the analysis presented here is sensitive to the energy dependence of the EBL thus providing a valuable diagnostic tool. This can be assessed by taking differences of TS_0 values in Table 3. For example the shape (not the normalization) of the optical depth curve as derived by Domínguez et al. (2011) is better than that of the "high-UV"

model of Kneiske et al. (2004) at $\Delta TS_0 = 10.4$. However, because the models are not nested, one needs to calibrate the probability of observing $\Delta TS_0 = 10.4$, or larger, by chance. We used Monte Carlo simulations of a set of 22 GRBs whose spectra have been attenuated by the EBL as predicted by the high-UV model Kneiske et al. (2004). Figure 6 shows the distribution of ΔTS_0 defined as the difference between the TS_0 produced with the Kneiske et al. (2004) high-UV model and the Domínguez et al. (2011) model. We derive that a $\Delta TS_0 > 10.4$ is observed in $\sim$1% of the cases corresponding to a 3σ evidence that the shape of the optical depth is better represented by the Domínguez et al. (2011) model rather than the high-UV model of Kneiske et al. (2004). This and Figure 5 show that the LAT is mostly sensitive to the EBL in the UV band, which is traditionally a very difficult component to model and understand because of the absorption of light in star-forming galaxies (Helgason & Kashlinsky 2012).

We have shown for the first time that a combined sample of GRBs can be used as an excellent probe of the EBL. The analysis presented here is based on the relatively small sample of 22 GRBs with known redshifts. However, if we scale the significance of the EBL attenuation by the number of sources, GRBs appear to have more constraining power than the BL Lacs used in Ackermann et al. (2012). This is due to their more simple intrinsic spectrum and high signal-to-noise spectra that are accumulated over a very short time, as well as higher redshift as compared to BL Lacs in Ackermann et al. (2012). Thus, it is desirable to extend our analysis to a larger burst sample underlining the importance of obtaining redshift determinations for future GRBs.

The authors acknowledge the comments of the referee. We acknowledge the support of NSF and NASA through grants AST-1715256 and 80NSSC17K0506 respectively. The *Fermi* LAT Collaboration acknowledges generous ongoing support from a number of agencies and institutes that have supported both the development and the operation of the LAT as well as scientific data analysis. These include the National Aeronautics and Space Administration and the Department of Energy in the United States, the Commissariat à l'Energie Atomique and the Centre National de la Recherche Scientifique/Institut National de Physique Nucléaire et de Physique des Particules in France, the Agenzia Spaziale Italiana and the Istituto Nazionale di Fisica Nucleare in Italy, the Ministry of Education, Culture, Sports, Science and Technology (MEXT), High Energy Accelerator Research Organization (KEK) and Japan Aerospace Exploration Agency (JAXA) in Japan, and the K. A. Wallenberg Foundation, the Swedish Research Council and the Swedish National Space Board in Sweden.

Additional support for science analysis during the operations phase is gratefully acknowledged from the Istituto Nazionale di Astrofisica in Italy and the Centre National d'Études Spatiales in France. This work performed in part under DOE Contract DE-AC02-76SF00515.

A.D. thanks the support of the Juan de la Cierva program from the Spanish MEC.

Facility: Fermi.

ORCID iDs

M. Ajello https://orcid.org/0000-0002-6584-1703
N. Omodei https://orcid.org/0000-0002-5448-7577
D. H. Hartmann https://orcid.org/0000-0002-8028-0991
A. Domínguez https://orcid.org/0000-0002-3433-4610
V. S. Paliya https://orcid.org/0000-0001-7774-5308
K. Helgason https://orcid.org/0000-0002-4326-9144
M. Meyer https://orcid.org/0000-0002-0738-7581

References

Abdo, A. A., Ackermann, M., Ajello, M., et al. 2009a, ApJL, 706, L138
Abdo, A. A., Ackermann, M., Arimoto, M., et al. 2009b, Sci, 323, 1688
Abramowski, A., Acero, F., Aharonian, F., et al. 2013, A&A, 550, A4
Acero, F., Ackermann, M., Ajello, M., et al. 2016, ApJS, 223, 26
Ackermann, M., Ajello, M., Allafort, A., et al. 2012, Sci, 338, 1190
Ackermann, M., Ajello, M., Allafort, A., et al. 2013a, ApJS, 209, 34
Ackermann, M., Ajello, M., Asano, K., et al. 2011, ApJ, 729, 114
Ackermann, M., Ajello, M., Asano, K., et al. 2013b, ApJS, 209, 11
Ackermann, M., Ajello, M., Asano, K., et al. 2013c, ApJS, 209, 11
Ackermann, M., Ajello, M., Atwood, W. B., et al. 2016, ApJS, 222, 5
Adams, F. C., Freese, K., Laughlin, G., Schwadron, N., & Tarlé, G. 1997, ApJ, 491, 6
Ahnen, M. L., Ansoldi, S., Antonelli, L. A., et al. 2016, A&A, 590, A24
Band, D., Matteson, J., Ford, L., et al. 1993, ApJ, 413, 281
Biteau, J., & Williams, D. A. 2015, ApJ, 812, 60
Bond, J. R., Carr, B. J., & Hogan, C. J. 1986, ApJ, 306, 428
Bouwens, R. J., Illingworth, G. D., Oesch, P. A., et al. 2015, ApJ, 803, 34
de Palma, F., Bissaldi, E., Tajima, H., et al. 2009, GCN, 9872
Domínguez, A., & Ajello, M. 2015, ApJL, 813, L34
Domínguez, A., Finke, J. D., Prada, F., et al. 2013, ApJ, 770, 77
Domínguez, A., & Prada, F. 2013, ApJL, 771, L34
Domínguez, A., Primack, J. R., Rosario, D. J., et al. 2011, MNRAS, 410, 2556
Driver, S. P., Andrews, S. K., Davies, L. J., et al. 2016, ApJ, 827, 108
Dwek, E., Arendt, R. G., & Krennrich, F. 2005, ApJ, 635, 784
Dwek, E., & Krennrich, F. 2013, APh, 43, 112
Dwek, E. 2014, AAS Meeting, 224, 401.01
Essey, W., Ando, S., & Kusenko, A. 2011, APh, 35, 135
Essey, W., & Kusenko, A. 2010, APh, 33, 81
Finke, J. D., Razzaque, S., & Dermer, C. D. 2010, ApJ, 712, 238
Franceschini, A., Rodighiero, G., & Vaccari, M. 2008, A&A, 487, 837
Furniss, A., Williams, D. A., Danforth, C., et al. 2013, ApJL, 768, L31
Ghisellini, G., Della Ceca, R., Volonteri, M., et al. 2010, MNRAS, 405, 387
Gilmore, R. C. 2012, MNRAS, 420, 800
Gilmore, R. C., Madau, P., Primack, J. R., Somerville, R. S., & Haardt, F. 2009, MNRAS, 399, 1694
Gilmore, R. C., Somerville, R. S., Primack, J. R., & Domínguez, A. 2012, MNRAS, 422, 3189
Gould, R. J., & Schréder, G. P. 1967a, PhRv, 155, 1408
Gould, R. J., & Schréder, G. P. 1967b, PhRv, 155, 1404
Greiner, J., Clemens, C., Krühler, T., et al. 2009, A&A, 498, 89
Guiriec, S., Gehrels, N., McEnery, J., Kouveliotou, C., & Hartmann, D. H. 2017, ApJ, 846, 138
Hartmann, D. H. 2007, in AIP Conf. Ser. 921, The First GLAST Symp., ed. S. Ritz, P. Michelson, & C. A. Meegan (New York: AIP), 24
Hauser, M. G., Arendt, R. G., Kelsall, T., et al. 1998, ApJ, 508, 25
Hauser, M. G., & Dwek, E. 2001, ARA&A, 39, 249
Helgason, K., & Kashlinsky, A. 2012, ApJL, 758, L13
Horns, D., & Meyer, M. 2012, JCAP, 2, 33
Inoue, Y., Inoue, S., Kobayashi, M. A. R., et al. 2013, ApJ, 768, 197
Inoue, Y., Tanaka, Y. T., Madejski, G. M., & Domínguez, A. 2014, ApJL, 781, L35
Kashlinsky, A. 2005a, PhR, 409, 361
Kashlinsky, A. 2005b, ApJL, 633, L5
Kashlinsky, A., Arendt, R. G., Ashby, M. L. N., et al. 2012, ApJ, 753, 63
Kashlinsky, A., Arendt, R. G., Mather, J., & Moseley, S. H. 2005, Natur, 438, 45
Keenan, R. C., Barger, A. J., Cowie, L. L., & Wang, W.-H. 2010, ApJ, 723, 40
Kneiske, T. M., Bretz, T., Mannheim, K., & Hartmann, D. H. 2004, A&A, 413, 807
Kneiske, T. M., & Dole, H. 2010, A&A, 515, A19
Kumar, P., & Barniol Duran, R. 2009, MNRAS, 400, L75
Kumar, P., & Barniol Duran, R. 2010, MNRAS, 409, 226
Madau, P., Ferguson, H. C., Dickinson, M. E., et al. 1996, MNRAS, 283, 1388
Madau, P., & Pozzetti, L. 2000, MNRAS, 312, L9
Matsumoto, T., Matsuura, S., Murakami, H., et al. 2005, ApJ, 626, 31
Matsuoka, Y., Ienaka, N., Kawara, K., & Oyabu, S. 2011, ApJ, 736, 119

Mattila, K., Väisänen, P., Lehtinen, K., von Appen-Schnur, G., & Leinert, C. 2017, MNRAS, 470, 2152
Mattox, J. R., Bertsch, D. L., Chiang, J., et al. 1996, ApJ, 461, 396
Maurer, A., Raue, M., Kneiske, T., et al. 2012, ApJ, 745, 166
Mazin, D., Domínguez, A., Fallah Ramazani, V., et al. 2017, in AIP Conf. Ser. 1792, 6th Int. Symp. on High Energy Gamma-Ray Astronomy (New York: AIP), 050037
Nikishov, A. I. 1961, JETP, 14, 394
Orr, M. 2011, Proc. ICRC, 8, 121
Primack, J. R., Bullock, J. S., & Somerville, R. S. 2005, in AIP Conf. Ser. 745, High Energy Gamma-Ray Astronomy, ed. F. A. Aharonian, H. J. Völk, & D. Horns (New York: AIP), 23
Raue, M., Kneiske, T., & Mazin, D. 2009, A&A, 498, 25
Scully, S. T., Malkan, M. A., & Stecker, F. W. 2014, ApJ, 784, 138
Stecker, F. W., Malkan, M. A., & Scully, S. T. 2006, ApJ, 648, 774
Stecker, F. W., Malkan, M. A., & Scully, S. T. 2012, ApJ, 761, 128
Stecker, F. W., Scully, S. T., & Malkan, M. A. 2016, ApJ, 827, 6
Tam, P.-H. T., Tang, Q.-W., Hou, S.-J., Liu, R.-Y., & Wang, X.-Y. 2013, ApJL, 771, L13
Tang, Q.-W., Peng, F.-K., Wang, X.-Y., & Tam, P.-H. T. 2015, ApJ, 806, 194
Vianello, G., Omodei, N. & Fermi/LAT Collaboration 2015, arXiv:1502.03122
Vianello, G., Omodei, N. & Fermi LAT Collaboration 2016, in American Astronomical Society Meeting Abstracts 227, 41601
Wang, X.-Y., He, H.-N., Li, Z., Wu, X.-F., & Dai, Z.-G. 2010, ApJ, 712, 1232
Zemcov, M., Smidt, J., Arai, T., et al. 2014, Sci, 346, 732
Zhang, B.-B., Zhang, B., Liang, E.-W., et al. 2011, ApJ, 730, 141